Inorg. Chem. **2007**, *46*, 5942–5948

First Ruthenium Complex of Glyoxalbis(*N*-phenyl)osazone ($L^{NHPh}H_2$): Synthesis, X-ray Structure, Spectra, and Density Functional Theory Calculations of $(L^{NHPh}H_2)Ru(PPh_3)_2Cl_2$

Amit Saha Roy,[†] Heikki M. Tuononen,[‡] Sankar P. Rath,[§] and Prasanta Ghosh*[,†]

Departments of Chemistry, R. K. Mission Residential College, Narendrapur, Kolkata-103, India, University of Jyväskylä, P.O. Box 35, FI-40014, Jyväskylä, Finland, and Indian Institute of Technology Kanpur, Kanpur-208016, India

Received February 14, 2007

The first ruthenium complex containing the parent osazone ligand, glyoxalbis(*N*-phenyl)osazone ($L^{NHPh}H_2$), is reported. The complex $(L^{NHPh}H_2)Ru(PPh_3)_2Cl_2$ (**1**) was characterized with mass, IR, ^1H NMR, and UV–vis spectroscopy as well as with theoretical calculations. Density functional theory calculations on the model compound $(L^{NHPh}H_2)Ru(PMe_3)_2Cl_2$ (**2**) reproduce the geometrical features observed for **1** and verify that it formally contains a ruthenium(II) metal center coordinated by a neutral osazone. Subsequent bonding analyses identify π-interactions between the occupied orbitals of the metal fragment and the LUMO of the osazone, which results in transfer of approximately 0.3 electrons from the metal to the ligand. The complex **1** absorbs strongly at 405 nm, which is assigned to a ruthenium-to-ligand charge-transfer band on the basis of results of theoretical calculations. Complex **1** is also electroactive and displays a single one-electron oxidation wave at 0.39 V; coulometric oxidation gives the oxidized species $[\mathbf{1}]^+$ as a $[PF_6]^-$ salt. Simulation of the EPR spectra of $[\mathbf{1}][PF_6]$, a one-electron paramagnetic species, affords **g**-tensor parameters $g_x = 2.2649$, $g_y = 2.0560$, and $g_z = 1.9064$ consistent with a ruthenium(III) description for $[\mathbf{1}]^+$, thereby confirming a metal-centered redox reaction.

1. Introduction

Complexes containing a diimine fragment, LH_2, coordinated to a metal center are of topical interest because of their numerous photophysical and catalytic activities.[1] The lone pairs of the nitrogen atoms and the π-electrons of the C=N bonds allow LH_2 ligands to act as efficient electron donors, which facilitates their coordination to metals using two, four, or (in rare occasions) as much as eight[2] electrons. In addition, the identities of the two substituents on the N=C−C=N backbone can also be varied, allowing for the steric and electronic properties of the ligand to be fine-tuned. The diimine ligand is also redox-active and readily accepts an electron to its low-lying lowest unoccupied molecular orbital (LUMO) thereby undergoing a one-electron reduction to form a diimine anion radical.[3]

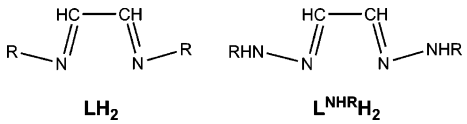

LH_2 $L^{NHR}H_2$

In contrast to the extremely versatile nature of LH_2 ligands in coordination complexes, the diimine fragment in osazones, $L^{NHR}H_2$, behaves chemically differently and, consequently, the coordination chemistry of this ligand is more limited in scope: so far only a few transition metal complexes of

* To whom correspondence should be addressed. E-mail: ghoshp_chem@yahoo.co.in. Phone: +91-33-2477-2205.
[†] R. K. Mission Residential College.
[‡] University of Jyväskylä.
[§] Indian Institute of Technology Kanpur.

(1) (a) Adams, C. J.; Fey, N.; Weinstein J. A. *Inorg. Chem.* **2006**, *45*, 6105. (b) Clarke, M. J. *Coord. Chem. Rev.* **2003**, *236*, 207. (c) Fox, M. A. *Synthetic Application of Photocatalytic oxidation and reduction reaction of organic reaction on Irradiated Semiconductor Surfaces*; Wiley-VCH: New York, 2001; Vol. 1. (d) Roundhill, D. M. *Photochemistry and Photophysics of Metal Complexes*; Plenum Press: New York, 1994. (e) Forster, R. J.; Keyes, T. E.; Vos, J. G. *Interfacial Supramoleculer Assemblies*; Wiley: London, New York, 2003; Chapter 6. (f) Gibson, V. C.; Tomov, A.; Wass, D. F.; White, A. J. P.; Williams, D. J. *Dalton Trans.* **2002**, 2261. (g) Wik, B. J.; Lersch, M.; Krivokapic, A.; Tilset, M. *J. Am. Chem. Soc.* **2006**, *128*, 2682. (h) Rix, F.; Brookhardt, M. *J. Am. Chem. Soc.* **1995**, *117*, 1137. (i) Mohring, M.; Fink, G. *Angew. Chem., Int. Ed. Engl.* **1985**, *97*, 982. (j) Kaim, W.; Kowaldt, F. H.; Goddard, R.; Kruger, C. *Angew. Chem., Int. Ed. Engl.* **1978**, *17*, 466.

(2) Keijsper, J.; van Koten, G.; Vrleze, K.; Zoutberg, M.; Stam, C. H. *Organometallics* **1985**, *4*, 1306.

10.1021/ic070294q CCC: $37.00
Published on Web 06/27/2007

osazones have been reported in literature.[4] There are two main reasons which have hindered the use of osazone as a coordinating ligand in metal complexes: (i) Osazones of the type $L^{NHR}H_2$ contain a reactive ═N−NH−R fragment which readily undergoes chemical transformations.[4] (ii) In the presence of protons and oxidizing agents, osazones are easily oxidized to osotriazoles.[5] Thus, all of the metal complexes of osazone currently reported in the literature contain only ligands of the type $L^{NHR}R_2$, i.e., in which the hydrogen atoms in the diimine fragment have been replaced with bulkier organic groups. So far there has not been a single report of a coordination compound containing the parent osazone ligand, $L^{NHR}H_2$, in which hydrogen atoms at both amino nitrogen and diimine carbon centers are retained. Because of their diimine fragments, osazones hold potential as useful ligands in metal complexes functioning as luminophores, probes, photosensitizers, and photoinitiators of radical reactions.[1,2] For this reason the development of osazone ligand chemistry represents a valuable objective.

Herein we respond to the above challenge by reporting the synthesis, X-ray crystal structure, and spectral features of $(L^{NHPh}H_2)Ru(PPh_3)_2Cl_2$ (**1**), the first transition metal complex containing the phenyl-substituted parent osazone ligand $L^{NHPh}H_2$. The molecular structure of complex **1** makes it a very interesting system also from a chemical point of view as ruthenium−diimine complexes are known to display tunable photochemical properties which may be varied out by independent replacement of the auxiliary ligands or by careful fine-tuning of the electronic structure of the diimine fragment.[6] Hence, the effect of the two NHR groups in the coordinated diimine fragment of **1** on the photophysical, redox, and bonding properties of the ligand are characterized using a combination of spectroscopic and theoretical methods. The bonding features of the complex are also discussed on the basis of its determined X-ray crystal structure, and a theoretical, molecular orbital based rationalization to the observed binding of the ligand fragment in **1** is given.

2. Experimental Section

2.1. Synthesis. 2.1.1. $Ru(PPh_3)_2Cl_2$. $Ru(PPh_3)_2Cl_2$ was prepared by an appropriate literature procedure.[7]

2.1.2. Glyoxalbis(*N*-phenyl)osazone. To a 40% aqueous solution of glyoxal (5 mmol) was added phenylhydrazine (10 mmol) with stirring. Immediately a yellow solid was formed. To the solid was added methanol (15 mL), and the yellow suspension was stirred for 0.5 h at 20 °C. The suspension was filtered and dried in air. Yield: 1100 mg (91% with respect to glyoxal). Mass spectrum (EI): *m*/*z* 238. ^{1}H NMR ($CDCl_3$, δ): 12.16 (s, 2H, NH), 7.63 (s, 2H, N═CH), 7.55 (d, 2H, Ph), 7.38−6.88 (m, 6H, Ph), 6.63 (d, 2H, Ph). Anal. Calcd for $C_{14}H_{14}N_4$: C, 70.58; H, 5.80; N, 23.50. Found: C, 70.46; H, 5.64; N, 23.10. IR (KBr): ν = 3305, 3292 (s) 1598 (vs), 1567 (vs), 1505 (vs) 1486 (vs), 1253 (vs), 1121 (vs), 752 (vs), 692 (vs), 513 (s) cm^{-1}.

2.1.3. $(L^{NHPh}H_2)Ru(PPh_3)_2Cl_2$. To a hot solution of glyoxalbis(*N*-phenyl)osazone ligand (0.4 mmol) in absolute ethanol (30 mL) was added $Ru(PPh_3)_2Cl_2$ (0.1 mmol), and the reaction mixture was refluxed for 45 min (78 °C). A red crystalline solid separated out. The mixture was cooled to 20 °C and filtered, and the residue was dried in air. Yield: 85 mg (91% with respect to ruthenium). Mass spectrum (ESI, positive ion, CH_2Cl_2): *m*/*z* 899.61, $\{\mathbf{1} - Cl\}^+$. ^{1}H NMR ($CDCl_3$, δ): 8.83, 8.68 (s, 2H, NH), 8.3 (s, 1H, N═CH), 5.95 (d, 4H, Ph), 7.71−6.78 (m, 37H, PPh_3, Ph, and N═CH). Anal. Calcd for $C_{50}H_{44}Cl_2N_4P_2Ru$: C, 64.24; H, 4.74; N, 5.99. Found: C, 63.96; H, 4.54; N, 5.90. IR (KBr): ν = 3225, 3214(m) 1595 (m), 1491 (s), 1433 (vs), 1093 (s), 695 (vs), 519 (vs) cm^{-1}.

2.2. X-ray Crystallographic Data Collection and Refinement of the Structures. Single crystals for X-ray structure determination were grown by diffusion of *n*-hexane to the dark red dichloromethane solution of **1**. Single-crystal X-ray data were collected at −173 °C on a Bruker SMART APEX CCD diffractometer using graphite-monochromated Mo Kα radiation (λ = 0.710 73 Å). The linear absorption coefficients, scattering factors for the atoms, and the anomalous dispersion corrections were taken from *International Tables for X-ray Crystallography*. The data integration and reduction were processed with SAINT software.[8] An absorption correction was applied.[9] The structure was solved by direct methods using SHELXS-97 and was refined on F^2 by full-matrix least-squares technique using the SHELXL-97 program package.[10] Non-hydrogen atoms were refined anisotropically. In the refinement, hydrogen atoms were treated as riding atoms using SHELXL default parameters. Crystallographic data of compound **1** are listed in Table 1.

2.3. Computational Details. Density functional theory (DFT) calculations were performed for the model system $(L^{NHPh}H_2)Ru(PMe_3)_2Cl_2$ (**2**) and its hydrogen-substituted analogue, as well as the one-electron oxidized $[\mathbf{2}]^+$ and reduced $[\mathbf{2}]^-$ species. The calculations utilized a combination of the hybrid PBE1PBE ex-

(3) See, for example: (a) Cloke, F. G. N.; Dalby, C. I.; Henderson, M. J.; Hitchcock, P. B.; Kennard, C. H. L.; Lamb, R. N.; Raston, C. L. *J. Chem. Soc., Chem. Commun.* **1990**, 1394. (b) Cloke, F. G. N.; Hanson, G. R.; Henderson, M. J.; Hitchcock, P. B.; Kennard, C. H. L.; Raston, C. L. *J. Chem. Soc., Chem. Commun.* **1989**, 1002. (c) Pott, T.; Jutzi, P.; Neumann, B.; Stammler, H. G. *Organometallics* **2001**, *20*, 1965. (d) Baker, R. J.; Farley, R. D.; Jones, C.; Mills, D. P.; Kloth, M.; Murphy, D. M. *Chem.—Eur. J.* **2005**, *11*, 2972. (e) Ghosh, P.; Bill, E.; Weyhermuller, T.; Neese, F.; Wieghardt, K. *J. Am. Chem. Soc.* **2003**, *125*, 1293. (f) Gardiner, M. G.; Hanson, G. R.; Henderson, M. J.; Lee, F. C.; Raston, L. C. *Inorg. Chem.* **1994**, *33*, 2456. (g) Corvaja, C.; Pasimeni, L. *Chem. Phys. Lett.* **1976**, *39*, 261. (h) Kaupp, M.; Stoll, H.; Preuss, H.; Kaim, W.; Stahl, T.; van Koten, G.; Wissing, E.; Smeets, W. J. J.; Spek, A. L. *J. Am. Chem. Soc.* **1991**, *113*, 5606. (i) Richter, S.; Daul, C.; Zelewsky, A. *Inorg. Chem.* **1976**, *15*, 943.

(4) See, for example: (a) Caglioti, L.; Cattalini, L.; Ghedini, M.; Gasparrini F.; Vigato, P. A. *J. Chem. Soc., Dalton Trans.* **1972**, 514. (b) Caglioti, L.; Cattalini, L.; Gasparrini F.; Ghedini, M.; Paolucci, G.; Vigato, P. A. *Inorg. Chim. Acta* **1973**, 538. (c) Maresca, L.; Natile, G.; Cattalini L. *J. Chem. Soc., Dalton Trans.* **1975**, 1601. (d) Maresca, L.; Natile, G.; Calligaris, M.; Delise, P.; Randaccio, L. *J. Chem. Soc., Dalton Trans.* **1976**, 2386. (e) Bolger, J. A.; Ferguson, G.; James, J. P.; Long, C.; McArdle, P.; Vos, J. G. *J. Chem. Soc., Dalton Trans.* **1993**, 1577. (f) Ammendola, P.; Ciajolo, M. R.; Panunzi, A.; Tuzi, A. *J. Organomet. Chem.* **1983**, *254*, 389. (g) Bavoso, A.; Funicello, M.; Morelli, G.; Pavone, V. *Acta Crystallogr.* **1984**, *C40*, 2035. (h) Mail, R. E.; Garralda, M. A.; Hernández, R.; Ibarlucea, L.; Pinilla, E.; Torres, M. R.; Zarandona, M. *Eur. J. Inorg. Chem.* **2005**, 1671. (i) Bikrani, M.; Mail, R. E.; Garralda, M. A.; Ibarlucea, L.; Pinilla, E.; Torres, M. R. *J. Organomet. Chem.* **2000**, *601*, 311.

(5) Hassan, E. K.; Pawel, C.; Christian, S. *Carbohydr. Res.* **1992**, *224*, 327.

(6) See, for example: (a) van Slageren, J.; Hartl, F.; Stufkens, D. J.; Martino, D. M.; van Willigen, H. *Coord. Chem. Rev.* **2000**, *208*, 309. (b) van Slageren, J.; Stufkens, D. J. *Inorg. Chem.* **2001**, *40*, 277.

(7) Stephenson, T. A.; Wilkinson, G. *J. Inorg. Nucl. Chem.* **1996**, *28*, 945.

(8) *SAINT+*, 6.02 ed.; Bruker AXS: Madison, WI, 1999.

(9) Sheldrick, G. M. *SADABS 2.0. Program for Empirical Absorption Correction of Area Detector Data*; University of Göttingen: Göttingen, Germany, 2000.

(10) Sheldrick, G. M. *SHELXL-97: Program for Crystal Structure Refinement*; University of Göttingen: Göttingen, Germany, 1997.

Table 1. Crystallographic Data for $(L^{NHPh}H_2)Ru(PPh_3)_2Cl_2$ (**1**)

formula	$C_{50}H_{44}Cl_2N_4P_2Ru$	T, K	100(2)
fw	934.80	ρ_{calcd}, g cm^{-3}	1.454
space group	$P2_1/n$	reflcns collcd/$2\theta_{max}$	25 940
a, Å	14.4605(10)	unique reflcns/$I > 2\sigma(I)$	9296
b, Å	21.1321(14)	no. of params	532
c, Å	14.7606(10)	λ, Å/μ(Mo Kα), cm^{-1}	0.710 73/0.690
β, deg	108.7730(10)	R_1[a]/GOF[b]	0.0444/0.929
V, Å^3	4270.6(5)	wR_2[c] ($I > 2\sigma(I)$)	0.0893
Z	4	resid density, e Å^{-3}	1.009

[a] Observation criterion: $I > 2\sigma(I)$. $R_1 = \Sigma||F_o| - |F_c||/\Sigma|F_o|$. [b] GOF = $[\Sigma[w(F_o^2 - F_c^2)^2]/(n-p)]^{1/2}$. [c] $wR_2 = [\Sigma[w(F_o^2 - F_c^2)^2]/\Sigma[w(F_o^2)^2]]^{1/2}$, where $w = 1/\sigma^2(F_o^2) + (aP)^2 + bP$ ($P = (F_o^2 + 2F_c^2)/3$).

change correlation functional[11] with the Ahlrichs' triple-ζ valence basis set augmented by polarization functions (def2-TZVP);[12] for ruthenium, the corresponding ECP basis set was used. Vibrational analyses were conducted to ensure that all optimized structures correspond to true minima in the potential energy hypersurface. The full optimized geometry of $(L^{NHPh}H_2)Ru(PMe_3)_2Cl_2$ is given in the Supporting Information in mol2 format. Geometry optimizations and frequency calculations were performed with the Turbomole 5.9 program package,[13a] whereas ADF 2006.01b[13b] was used in fragment molecular orbital analyses (PBE1PBE/TZ2P level of theory with scalar relativistic ZORA treatment of all electrons).

3. Results and Discussion

3.1. Characterization and Molecular Structure. The synthesis of the ligand $L^{NHPh}H_2$ has been reported previously,[14] but it was prepared by a modified procedure (see above). The compound **1** was synthesized in high yield by reacting the $L^{NHPh}H_2$ ligand with $Ru(PPh_3)_2Cl_2$ in boiling ethanol under air. The ^{1}H NMR spectrum of **1** in $CDCl_3$ confirmed the presence of both NH protons which appear as two singlets at $\delta = 8.83$ and 8.68 ppm. For comparison, the NH protons of a free $L^{NHPh}H_2$ ligand resonate at $\delta = 12.16$ ppm in $CDCl_3$ but appear at $\delta = 7.65$ ppm in DMSO-d_6.[14] Some of the aromatic protons in **1** are shielded by the diamagnetic ring current of the phenyl rings of the two PPh_3 ligands and, therefore, resonate at higher field. The trend in NH resonance frequency between the complex and the free ligand is consistent with the binding of the metal ion to the adjacent imine nitrogen atoms in the former species. The effect of complex formation is also clearly visible in the IR spectrum: the N−H stretching vibrations of the free ligand appear at 3305 and 3295 cm^{-1} while those of the complex **1** are observed at slightly lower frequencies, 3225 and 3214 cm^{-1}.

The complex **1** crystallizes in a $P2_1/n$ space group. The molecular structure of **1** with the atomic numbering scheme is depicted in Figure 1, and the relevant bond parameters

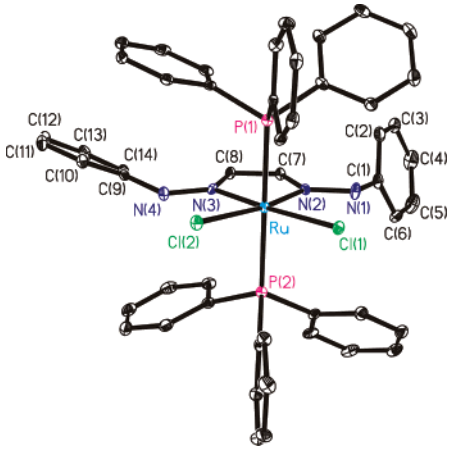

Figure 1. Single-crystal X-ray structure of **1**. (Hydrogen atoms are omitted for clarity.)

Table 2. Selected Bond Distances (Å) and Angles (deg) of **1**

Ru−N(2)	2.023(3)	Ru−N(3)	2.026(3)
Ru−P(1)	2.3830(8)	Ru−P(2)	2.3636(9)
Ru−Cl(1)	2.4379(8)	Ru−Cl(2)	2.4563(8)
N(1)−N(2)	1.374(3)	N(2)−C(7)	1.308(4)
C(7)−C(8)	1.408(4)	C(8)−N(3)	1.316(4)
N(3)−N(4)	1.349(3)	N(4)−C(9)	1.410(4)
C(1)−C(2)	1.400(4)	C(2)−C(3)	1.362(5)
C(3)−C(4)	1.382(5)	C(4)−C(5)	1.368(5)
C(5)−C(6)	1.369(5)	C(6)−C(1)	1.395(4)
N(1)−C(1)	1.425(4)	C(9)−C(10)	1.390(4)
C10−C(11)	1.381(4)	C(11)−C(12)	1.381(4)
C(12)−C(13)	1.375(5)	C(13)−C(14)	1.388(4)
C(9)−C(14)	1.383(4)		
N(2)−N(1)−C(1)	119.9(2)	C(8)−N(3)−N(4)	124.1(3)
C(7)−N(2)−N(1)	121.1(3)	N(3)−N(4)−C(9)	130.3(3)

are summarized in Table 2. The Ru−P(1), Ru−P(2), and Ru−Cl distances in **1** correspond to the reported Ru(II)−P[15] and Ru(II)−Cl[16] bond lengths in complexes with *trans*-$Ru(PPh_3)_2$ geometry. The diimine CC bond in **1** is considerably shorter than a typical single bond between two sp^2-hybridized carbon atoms, 1.47 Å, but not significantly different from CC bonds in closely related transition metal complexes with osazone-type ligands, 1.46 ± 0.03 Å (average value from 34 crystal structures found in the Cambridge Structural Database v5.28). The two NC bonds in **1** are only slightly elongated with respect to ideal nitrogen−carbon double bond length, 1.28 Å, and, thus, are typical for metal coordinated diimine fragments.

As already mentioned in the Introduction, it is a well-known fact that the diimine chromophore is electronically flexible and can readily accept excess electron density. There are two common mechanisms which operate in diimine metal complexes: (i) The CC bonding LUMO of the diimine can abstract an electron from the metal thereby forming an

(11) (a) Perdew, J. P.; Burke, K.; Ernzerhof, M. *Phys. Rev. Lett.* **1996**, *77*, 3865. (b) Perdew, J. P.; Burke, K.; Ernzerhof, M. *Phys. Rev. Lett.* **1997**, *78*, 1396. (c) Perdew, J. P.; Ernzerhof, M.; Burke, K. *J. Chem. Phys.* **1996**, *105*, 9982. (d) Ernzerhof, M.; Scuseria, G. E. *J. Chem. Phys.* **1999**, *110*, 5029.

(12) All basis sets were used as they are referenced in the Turbomole 5.9 internal basis set library. See: ftp://ftp.chemie.uni-karlsruhe.de/pub/ for the explicit basis set listings.

(13) (a) Turbomole 5.9: Ahlrichs, R.; Bär, M.; Häser, M.; Horn, H.; Kölmel, C. *Chem. Phys. Lett.* **1989**, *162*, 165. (b) *ADF2006.01b, SCM*; Theoretical Chemistry, Vrije Universiteit: Amsterdam, The Netherlands, 2006; http://www.scm.com.

(14) Gallucci, R. R. *J. Chem. Eng. Data* **1982**, *27*, 217.

(15) (a) Ghosh, P.; Chakravorty, A. *Inorg. Chem.* **1997**, *36*, 64. (b) Menon, M.; Pramanik, A.; Chattopadhyay, S.; Bag, N.; Chakravorty, A. *Inorg. Chem.* **1995**, *34*, 1361. (c) Pramanik, A.; Bag, N.; Chakravorty, A. *J. Chem. Soc., Dalton Trans.* **1992**, 97. (d) Sahajpal, A; Robinson, S. D.; Mazid, M. A.; Motevalli, M.; Hursthouse, M. B. *J. Chem. Soc., Dalton Trans.* **1990**, 2119.

(16) (a) Bag, N.; Choudhury, S. B.; Pramanik, A.; Lahiri, G. K.; Chakravorty, A. *Inorg. Chem.* **1990**, *29*, 1361. (b) Bag, N.; Choudhury, S. B.; Lahiri, G. K.; Chakravorty, A. *J. Chem. Soc., Chem. Commun.* **1990**, 1626. (c) Ghosh, P.; Bag, N.; Chakravorty, A. *Organometallics* **1996**, *15*, 3042.

anionic radical ligand.[3] (ii) If the orbital energies of the ligand and the metal fragment match, the formally unoccupied LUMO of the diimine fragment can contribute to MOs with ligand−metal π-bonding character, which in essence leads to transfer of electron density to atoms in the diimine backbone.[17,18] It can sometimes be difficult to differentiate which one of the two mechanisms operates in each particular case as they both give rise to structures with nearly identical geometrical parameters: the resulting complexes generally have diimine CC and CN bond lengths which are close to 1.40 and 1.33 Å, i.e., between that of single and double bond values.[3,17]

Considering the molecular structure established for complex **1**, the geometrical parameters of the osazone ligand are very close what one would expect if the complex contained a monoanionic diimine radical.[3] On the other hand, some related metal−diimine complexes with trans-σ-bonded ligands display similar bonding pattern in their diimine fragments solely due to orbital interactions.[17a,b] The significant difference between the two possibilities with respect to complex **1** is that the former mechanism leads to a structure which has internal singlet diradical character (a monoradical ligand coordinated to a Ru(III) center), whereas the latter one gives a complex with a pure singlet ground state. Hence, to establish unequivocally whether the geometrical features observed for the diimine ligand in **1** could be explained with either one of the above two mechanism, the bonding in **1** was inspected in detail using density functional theory (DFT) calculations and the fragment molecular orbital (FMO) method. We note that EPR spectroscopy cannot be used to identify between the two alternatives as no signal can be detected for molecules with singlet diradical ground states.

3.2. Molecular Orbital Analysis. To better understand the electronic structure and bonding properties of complex **1**, theoretical calculations were conducted for a model system ($L^{NHPh}H_2$) $Ru(PMe_3)_2Cl_2$ (**2**) in which the two triphenylphosphine groups are replaced with computationally much less demanding trimethylphosphines. The optimized bond parameters of the model complex **2** are in excellent agreement with results from crystal structure determination of **1**: the calculated values of some key parameters are Ru−N = 2.01 Å, N=C = 1.31 Å, C−C = 1.41 Å, N−N = 1.34 Å, −NRuN = 78.8°, −RuNC = 115.1°, and −NCC = 115.5°. Hence, the chosen level of theory accurately reproduces the bonding features observed for the diimine backbone of the osazone ligand in **1**.

The bonding in complex **2** was analyzed by using the FMO approach which investigates the orbital interactions between the osazone ligand and the metal fragment in detail. To simplify the MO figures in the orbital interaction diagram, we limit the discussion to the analysis of the fully unsubstituted system, i.e., $(L^{NH}{}_2H_2)Ru(PH_3)_2Cl_2$; results obtained for complex **2** are virtually identical at both qualitative and quantitative levels to the ones presented in below.

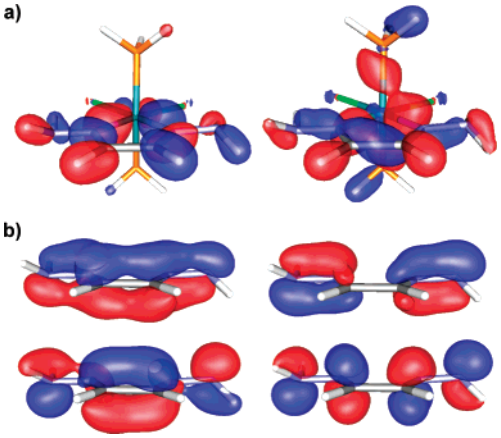

Figure 2. (a) Important σ-interactions between the ligand $L^{NH}{}_2H_2$ and the metal fragment $Ru(PH_3)_2Cl_2$ in **1**. (b) Occupied π MOs of the free $L^{NH}{}_2H_2$ ligand.

The fragment MO analysis revealed that the σ-symmetric interactions between the ligand and the metal fragment take place via ligand MOs 11a and 11b, which correspond to the two nitrogen lone pairs; the metal fragment participates in σ-type bonding primarily via three orbitals which are linear combinations of ruthenium d orbitals with either p orbitals of phosphorus or chlorine. The resulting MOs in the complex are pictured in Figure 2a. Such interactions are expected considering that the osazone ligand acts as a four-electron donor in the current case. The σ-bonding framework of the complex does not, however, reveal any interactions which would explain the observed geometrical features as electron density is transferred to the metal fragment from orbitals which are primarily lone pair in character. Hence, the π-system of the complex was analyzed in detail.

The free $L^{NH}{}_2H_2$ ligand has four occupied MOs predominantly π-like in character which correspond to eight electrons, four in two lone pairs and four in two C=N double bonds (see Figure 2b). As the two terminal amino centers are sp^3 hybridized in $L^{NH}{}_2H_2$ (and in $L^{NRH}H_2$), the nonplanarity of the ligand system does not allow full delocalization of π-electrons. However, some conjugation throughout the entire N−N=C−C=N−N backbone takes place as evidenced by the composition of the four orbitals in Figure 2b. When the $L^{NH}{}_2H_2$ ligand chelates a metal, its π-orbitals interact with the orbitals of the metal fragment. A FMO analysis conducted for the π-framework reveals that this results in a net transfer of electron density from the metal to the ligand via *back-bonding* interactions. The orbital which functions as the primary electron acceptor is the LUMO of the osazone ligand (orbital 12b), which interacts with the occupied orbitals 20b and 21b of the metal fragment: the percentage contribution of the ligand LUMO to the occupied MOs 31b (HOMO-2) and 32b (HOMO-4) in the complex is 5.3 and 10.6%, respectively. Hence, the formally empty CC bonding LUMO of the ligand accepts approximately 0.32

(17) See, for example: (a) Aarnts, M. P.; Wilms, M. P.; Peelen, K.; Fraanje, J.; Goubitz, K.; Hartl, F.; Stufkens, D. J.; Baerends, E. J.; Vicek, A. *Inorg. Chem.* **1996**, *35*, 5468. (b) Aarnts, M. P.; Hartl, F.; Peelen, K.; Stufjens, D. J.; Amatore, C.; Verpeaux, J.-N. *Organometallics* **1997**, *16*, 4686. (c) Makedonas, C.; Mitsopolou, C. A. *Eur. J. Inorg. Chem.* **2007**, 110.

(18) The interaction of diimine fragment with different metals has been analyzed in detail. See, for example: (a) Mealli, C.; Ienco, A.; Anillo, A.; García-Granda; Obeso-Rosete, R. *Inorg. Chem.* **1997**, *36*, 3724. (b) Anillo, A.; Garcia-Granda, S.; Obeso-Rosete, R.; Galindo, A.; Ienco, A.; Mealli, C. *Inorg. Chim. Acta* **2003**, *350*, 557.

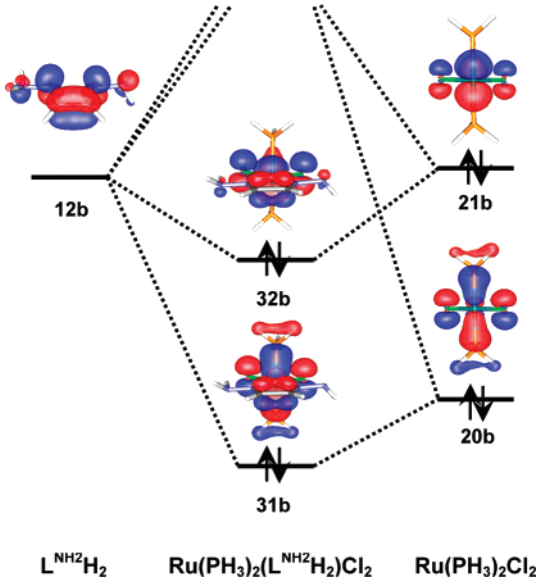

Figure 3. Important π-interactions between the ligand $L^{NH_2}H_2$ and the metal fragment $Ru(PH_3)_2Cl_2$ in **1**.

electrons—clearly a nonnegligible number—from the metal, which leads to the observed bond parameters in **1**. A pictorial representation of the above is shown in Figure 3, which includes an orbital correlation diagram of the important π-interactions.

The FMO analysis greatly enforces the interpretation that the complex **1** formally contains a neutral $L^{NHPh}H_2$ ligand and a Ru(II) center (low-spin d^6, $S = 0$). This view is backed up by SCF stability calculations conducted for **2** which show that the optimized solution obtained for the singlet ground state has no instabilities characteristic of an internal diradical character. In addition, the RuN bond lengths in the complex **1** show values which are atypical for strong bonding interactions involving a Ru(III) center and an anionic ligand but instead very characteristic for single bonds between a divalent Ru atom and a neutral donor ligand.

3.3. Electro- and Spectroelectrochemistry. Compound **1** is electroactive: its cyclic voltammogram in CH_2Cl_2 (0.20 M $[N(n\text{-}Bu)_4]PF_6$ supporting electrolyte, glassy carbon working electrode, scan rate 100 mV s^{-1}) at 20 °C displays a single reversible one-electron oxidation wave at 0.391 V referenced vs the ferrocenium/ferrocene couple (Fc^+/Fc). The one electron oxidation process observed in the cyclic voltammogram appears to be ruthenium-centered, and the coulometrically generated (at −20 °C) oxidized species[1][PF_6] was characterized by EPR and UV−vis spectroscopy (see below). No reduction wave typical for similar Ru−diimine complexes[17a,b] was observed up to −1.8 V (minimum potential allowed by the experimental setup), but one electron reduction at a more negative potential could result in formation of a diimine anion radical. This hypothesis is backed up by theoretical calculations, which indicate that complex **1** readily accepts an electron as the anion is found to be extremely stable species: [**2**]$^-$ is computationally approximately 115 kJ mol^{-1} lower in energy than the neutral complex. Another interesting feature revealed by the calculations is the predicted electron distribution in [**2**]$^-$: as the LUMO of the osazone ligand has p_π orbital contributions also from the two amino nitrogen atoms (see orbital 12b in Figure 3), the unpaired electron in [**2**]$^-$ becomes delocalized throughout the entire NNCCNN fragment, which could function to increase the stability of the paramagnetic radical.

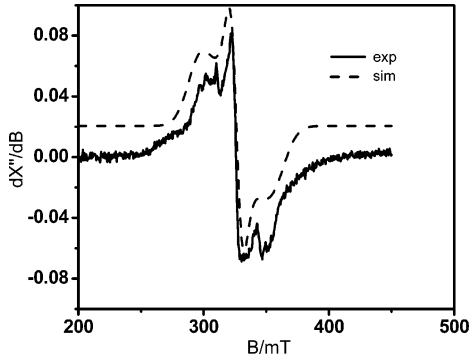

Figure 4. X-Band EPR spectrum of [**1**]$^+$ in frozen CH_2Cl_2 at −243 °C (frequency, 9.43 GHz; power, 2.5 × 10^{-6} mW; modulation amplitude, 8.0 G).

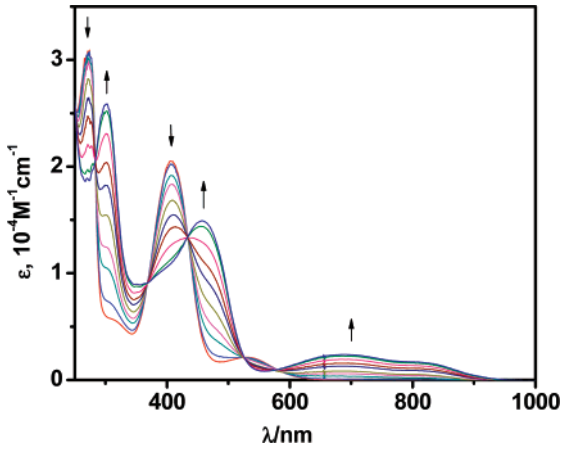

Figure 5. Spectral changes observed during coulometric oxidation of **1** to [**1**]$^+$ in CH_2Cl_2 (0.20 M $[N(n\text{-}Bu)_4]PF_6$) at −25 °C.

Table 3. Experimental UV−Vis Data for Complexes **1** and [**1**][PF_6]

complex	λ_{max} (nm) (ϵ (10^4 M^{-1} cm^{-1}))
1	534 (0.23), 406 (2.06), 318 (0.57), 272 (3.06), 237 (3.27)
[**1**][PF_6]	816 (0.16), 690 (0.23), 457 (1.50), 299 (2.50), 237 (3.30)

The X-band EPR spectrum of [**1**][PF_6] in CH_2Cl_2 solution at −243 °C yields a single broad resonance depicted in Figure 4, which confirms the paramagnetic nature of [**1**]$^+$ ($S = {}^1/_2$). From an approximate simulation of the frozen solution spectra, the following **g**-tensor parameters were deduced: $g_x = 2.2649$; $g_y = 2.0650$; $g_z = 1.9064$; $g_{iso} = 2.0241$. These parameters are consistent with a metal-centered oxidation, in good agreement with results of DFT calculations which showed that the highest occupied molecular orbital (HOMO) of **2** contains a significant contribution from ruthenium d orbitals.

The electronic spectra of both **1** and its electrochemically generated monocation [**1**][PF_6] measured at −25 °C are shown in Figure 5; relevant spectral data are summarized in Table 3. The brown solution of [**1**][PF_6] is stable only at low temperature and in an argon blanket atmosphere. The UV−vis spectrum monitored during the spectroelectrochemi-

Table 4. Calculated Excitation Energies and Assignments of Low-Lying Electronic Transitions of Complexes **2** and $[\mathbf{2}]^+$

complex	symmetry	energy (nm)[a]	significant contributions (>10%)	dominant type
2	a_1	392 (0.099)	HOMO-3 → LUMO (93%)	$d_{Ru} + p_{Cl} \rightarrow p^*_L$
	a_2	346 (0.027)	HOMO-5 → LUMO (98%)	$\pi_L \rightarrow \pi^*_L$
	b_2	566 (0.025)	HOMO → LUMO (62%)	$d_{Ru} + p_{Cl} + \pi_L \rightarrow \pi^*_L$
			HOMO-1 → LUMO (24%)	$d_{Ru} + p_{Cl} \rightarrow \pi^*_L$
			HOMO-2 → LUMO (13%)	$d_{Ru} + p_{Cl} \rightarrow \pi^*_L$
	b_3	390 (0.395)	HOMO-2 → LUMO (65%)	$d_{Ru} + p_{Cl} \rightarrow \pi^*_L$
			HOMO-1 → LUMO+6 (21%)	$d_{Ru} + p_{Cl} \rightarrow p_{Cl} + d_{Ru}$
	b_4	380 (0.189)	HOMO-1 → LUMO+6 (67%)	$d_{Ru} + p_{Cl} \rightarrow p_{Cl} + d_{Ru}$
			HOMO-2 → LUMO (19%)	$d_{Ru} + p_{Cl} \rightarrow \pi^*_L$
$[\mathbf{2}]^+$	a_2	877 (0.002)	SOMO β → LUMO β (68%)	$\pi_L \rightarrow d_{Ru} + \pi_{Cl}$
			SOMO-2 β → LUMO β (30%)	$d_{Ru} + p_{Cl} \rightarrow d_{Ru} + p_{Cl}$
	b_3	686 (0.002)	SOMO-4 β → LUMO β (51%)	$d_{Ru} \rightarrow d_{Ru} + p_{Cl}$
			SOMO-3 β → LUMO β (27%)	$d_{Ru} + p_{Cl} \rightarrow d_{Ru} + p_{Cl}$
			SOMO-5 β → LUMO β (20%)	$d_{Ru} + \pi_L \rightarrow d_{Ru} + p_{Cl}$
	b_6	423 (0.045)	SOMO-9 β → LUMO+1 β (37%)	$p_{Cl} \rightarrow \pi^*_L$
			SOMO β → LUMO+1 β (24%)	$\pi_L \rightarrow \pi^*_L$
			SOMO-1 α → LUMO+1 α (20%)	$\pi_L \rightarrow \pi^*_L$
			SOMO-2 β → LUMO+1 β (15%)	$d_{Ru} + p_{Cl} \rightarrow \pi^*_L$
	b_7	418 (0.076)	SOMO-9 β → LUMO β (57%)	$p_{Cl} \rightarrow d_{Ru} + p_{Cl}$
			SOMO-2 β → LUMO+1 β (18%)	$d_{Ru} + p_{Cl} \rightarrow \pi^*_L$

[a] Oscillator strengths are given in parentheses.

cal oxidation shows a clean isosbestic conversion. The parent complex **1** displays three absorbance maxima at 405, 272, and 237 nm in CH_2Cl_2. Upon oxidation of **1**, the strong band at around 400 nm is replaced by two bands of the paramagnetic cation at 450 and 690 nm. No emission bands were observed in the fluorescence spectrum measured for complex **1**, which indicates that the parent osazone ligand holds limited possibilities to be used in complexes with highly tunable photochemical properties; it will be of interest to study whether this property can be affected via selective substitution of the ligand in an analogical fashion as found for some structurally similar Ru−osazone complexes.[4b]

To better understand the optical spectrum measured for **1** and $[\mathbf{1}][PF_6]$, theoretical calculations were carried out for **2** and $[\mathbf{2}]^+$ at the TD-DFT level of theory; the results are collected in Table 4. Computational analysis of the absorption properties of **2** finds three high-intensity transitions between 380 and 390 nm all of which involve electron transfer from high-lying MOs having significant metal d orbital character to the ligand based unoccupied orbitals, primarily LUMO. Such transitions are very typical for a variety of Ru−diimine complexes and are, thus, assigned to the experimental band at around 400 nm.[4b,6,17a,b,19] The lower intensity band with an experimental band maximum at around 535 nm corresponds nicely with the calculated transition at 565 nm with 62% HOMO → LUMO character.

DFT calculations for the bare cation $[\mathbf{2}]^+$ indicate that the removal of electron from the HOMO of **2** does not lead to significant changes in geometry: the only notable difference is the elongation of Ru−N bonds by 0.07 Å to 2.08 Å as electron density is removed from an orbital with significant Ru d orbital character. The calculations show that the transition with primarily SOMO → LUMO character should be of low intensity and observed at the near-IR portion of the electromagnetic spectrum, close to 880 nm (see Table 4): this result corresponds reasonably well with the birth of a low-intensity band with an absorbance maximum at 816 nm to the UV−vis spectrum of **1** upon oxidation. The results of DFT calculations for $[\mathbf{2}]^+$ suggest that the second low-intensity band in the experimental spectrum of $[\mathbf{1}][PF_6]$ most likely has its origin in metal-centered excitations: both the calculated transition energy as well as the oscillator strength match with the properties of the transition observed in the experimental spectrum at 690 nm. Ligand-centered and ligand-to-metal type excitations with higher oscillator strengths are also found at around 420 nm (two transitions), which are in reasonable agreement with the most intense band observed in the high-energy side of the visible spectrum of $[\mathbf{1}][PF_6]$ at around 460 nm.

4. Conclusion

This study represents a significant addition to the coordination chemistry of simple organic ligands which contain a diimine chromophore by reporting the first ruthenium(II) complex of glyoxalbis(*N*-phenyl)osazone, $(L^{NHPh}H_2)Ru(PPh_3)_2Cl_2$ (**1**), in which two chlorine ions and triphenylphosphine groups act as coligands. The photophysical, redox, and bonding properties of the complex were characterized using a combination of spectroscopic and theoretical methods. The results demonstrate that $(L^{NHPh}H_2)Ru(PPh_3)_2Cl_2$ has electronic properties similar to those of its known diimine counterparts. In particular, complex **1** shows an UV−vis absorption spectrum with a high-intensity metal-to-ligand charge-transfer band typical for analogous Ru−diimine complexes; complex **1** is also electroactive and displays a single one-electron oxidation wave at 0.39 V. DFT-based bonding analyses showed that $(L^{NHPh}H_2)Ru(PPh_3)_2Cl_2$ exhibits moderately strong π-interactions which transfer approximately 0.32 electrons from the occupied orbitals of the ruthenium(II) fragment to the formally unoccupied LUMO of the osazone ligand. The encouraging results obtained in this study indicate that the hitherto unexplored coordination chemistry of osazone with 3d and 5d transition metals is a sought-after

(19) Adams, H.; Alsindi, W. Z; Davies, G. M.; Duriska, M. B.; Easun, T. L.; Fentony, H. E.; Herrera, J. M.; George, M. W.; Ronayne, K. L.; Sun, X. Z.; Towrie, M.; Ward, M. D. *Dalton Trans.* **2006**, 39.

objective. In addition, considering the facile synthesis of **1**, it will be of interest to examine the effect on different substituents to its electronic properties in more detail. The DFT predicted stability for the anionic metal complex $[\mathbf{1}]^-$ containing a paramagnetic osazone radical should also be verified experimentally.

Acknowledgment. This work was supported by the University Grants Commission (UGC), New Delhi, India. We are grateful to MPI-fur Bioanorganische Chemie, Muelheim, Germany, for spectroelectrochemical measurements. H.M.T thanks the Academy of Finland for financial support.

Supporting Information Available: X-ray crystallographic files for complex **1** as well as optimized coordinates for compound **2**. This material is available free of charge via the Internet at http://pubs.acs.org.

IC070294Q